Polymer Journal (2019) 51:547–558
https://doi.org/10.1038/s41428-018-0153-4

ORIGINAL ARTICLE

Effect of natural melanin nanoparticles on a self-healing cross-linked polyurethane

Xiaoyue Ma[1] · Chuanying Shi[1] · Xiaowen Huang[1] · Yang Liu[1] · Yanyan Wei[1]

Received: 18 July 2018 / Revised: 19 October 2018 / Accepted: 22 October 2018 / Published online: 13 February 2019

Abstract

Natural melanin nanoparticles (MNs) stripped from cuttlefishes were purified and characterized for the first time. The reactive groups (–OH or $–NH_2$) of the MNs at a concentration of 6.0 mmol/g react with isocyanate groups in pre-polyurethane (pre-PU) to form cross-links, further strengthening the self-healing of PU based on the reversible acylhydrazone bond that was synthesized for the first time in this study. Then, the performances of different mass fractions of self-healing PU modified with MNs (0.5, 1, 1.5, 2, 2.5 wt%) were characterized. We found that PU modified with 1.5 wt% of MNs showed better performance due to the adjustment of the micro-phase separation in PU, with the σ and ε values improved from 0.81 MPa and 405.44% to 2.75 MPa and 483.17%, respectively. Surprisingly, the self-healing efficiency, defined by the recovery of ε, was improved from 91.73% to 99.58% due to the strong interactions between the MNs and PU. The aim of this study was to perfectly combine the organic active fillers—melanin nanoparticles—with self-healing materials to enhance their performance.

Introduction

Polyurethane materials have a wide range of possible applications in aerospace, machinery, medicine, construction, and other engineering fields due to their excellent performances and desirable physical and mechanical properties [1]. These desirable properties include their broad reactive characteristics and ability to flexibly adjust their soft and hard segments [2]. Polyurethane materials can be endowed with a self-healing capability by introducing functional chemical bonds into the matrix [3]. These functional chemical bonds, especially reversible covalent bonds [4, 5], may exist in dimers of acylbenzofuran ketones [6], trisulfide esters [7], aryl boric acid esters [8], Diels–Alder bonds [9], acylhydrazone compounds [10], disulfide compounds [11], C–ON compounds [12], coumarin [13], or cinnamate [14]. These reversible covalent bonds can be stably distributed in polyurethane and play an important part in self-healing.

Among the reversible covalent bonds, acylhydrazone bonds have good thermal and solvent stability due to their strong bond energy and interactions with the matrix. Since they were first successfully used by Lehn [15] and co-workers to prepare dynamic covalent polymers, acylhydrazone bonds have been well developed in terms of material properties. Furthermore, self-healing materials based on acylhydrazone bonds can efficiently self-heal cracks under gentle conditions. In recent years, Deng et al. synthesized a cross-linked polymer based on acylhydrazone bonds and examined its self-healing behavior [16]. Self-healing process on the reversibility of the acylhydrazone bond occurred instantaneously after simply placing cracked gel plates in contact without using any external stimulus under ambient conditions [17]. The applicability of self-healing materials based on reversible covalent bonds, however, is restricted by their poor mechanical performance. Reversible covalent bonds have mostly been introduced into the system as elastomers or gels, which are all extremely soft with a linear or branched structure. Cross-linked networks based on acylhydrazone bonds and their self-healing properties in polyurethane elastomer have not been reported to date [18–20].

✉ Yanyan Wei
yywei@qust.edu.cn

[1] Key Laboratory of Rubber-plastics, Ministry of Education/ Shandong Provincial Key Laboratory of Rubber-plastics, School of Polymer Science and Engineering, Qingdao University of Science & Technology, Shandong, PR China

As science keeps pace with the times, systems for self-healing materials have undergone diverse development. Xu [21] found that the di-selenide bonds in 2,2,6,6-tetramethylpiperidin-1-yloxyl (TEMPO) were dynamic covalent bonds and that the materials based on the di-selenide bonds could undergo dynamic exchange reactions under mild conditions, such as irradiation with visible light. Bao [22] and her team synthesized materials that possess strong, elastic, and self-healing properties, which were achieved by networks of poly(dimethylsiloxane) polymer chains cross-linked by coordination complexes that consisted of 2,6-pyridinedicarboxamide ligands. The ligands were able to coordinate to ferric ions through the pyridyl rings of the 2,6-pyridinedicarboxamide or the nitrogen atoms and oxygen atoms of the carboxamide groups. The former interaction was strong enough to impose iron attachment to the ligands. The two other weak iron–ligand bonds were able to readily break and re-form, enabling reversible unfolding and refolding of the chains to achieve high stretch ability and a good self-healing capability, which makes the material useful in artificial muscle applications due to its ability to restore a high dielectric strength after recovering from mechanical damage. Self-healing materials that have a restoration mechanism have become more diverse; therefore, their practical and intelligent applications have gained increasing attention.

Polymer nanocomposites can endow polyurethane with extraordinary properties [23] and promote the reaction of reactive additives, such as graphene oxide (GO), chitosan or other natural nanoparticles, with the isocyanate group of polyurethane [24]. The chemical cross-links formed by the reaction will strengthen the interaction between nanocomposites and the PU matrix. Furthermore, functional polymer nanocomposites have been extensively used to improve PU performance [25, 26]. New research by Chen et al. from Jiangnan University claimed that the melanin nanocomposites from Sepia can remarkably enhance the tensile strength and toughness of polyurethane [27]. It was found that a suitable amount of melanin nanocomposites dispersed in the matrix can specifically link to the hard domains of PU [28]. Indeed, an improvement in the degree of phase separation caused by these links induced remarkable enhancements in the mechanical properties of PU. Although melanin is a widely distributed multifunctional biomacromolecule, its exact molecular structure and number of reactive functional groups (–OH, –NH–, $–NH_2$) remain poorly documented [29].

Melanin nanoparticles (MNs) were prepared from the ink bags of cuttlefish [30], centrifuged (20,000 rpm, 15 min), and ultrasonically washed several times to remove organic matter or dissolved inorganic matter. Then, clean MNs were collected by vacuum dehydration at 50 °C for 7 days. We characterized their morphology, particle size, and functional groups; evaluating the content of MNs added to the polyurethane, the subsequent reaction and the role MNs play in the matrix are the aims of this paper. Furthermore, we examined the molecular structure and size distribution of MNs to determine their applicability in other fields.

First, for the design of a new class of self-healing materials, a polyurethane elastomer based on acylhydrazone bonds was synthesized. The new hydroxyl terminated acylhydrazone compound was utilized as a cross-linker to combine the chains of trifunctional pre-polyurethane and bifunctional pre-polyurethane. Pre-polyurethanes were synthesized using commercially available polyhydric alcohol to fine-tune the soft and hard segments of the polyurethane systems [31, 32]. The new self-healing polyurethane materials have good mechanical properties and broader application prospects. MN-modified self-healing polyurethane was synthesized by a novel method, and the effect of melanin on the properties of polyurethane was investigated by a series of characterizations. Furthermore, the basic self-healing mechanism and corresponding mechanical properties were analyzed.

Experimental

Materials

Cuttlefish-bag (crude MNs) and diphenylmethane diisocyanate (MDI-50, Mn = 250.26) were purchased from Wanhua Chemical Group Co. Ltd. Bifunctional polyhydric alcohol, polycaprolactone polyol with trade name PCL-210 (hydroxyl value 110 mgKOH/g, Mn = 1000, Shenzhen Yisheng Co. Ltd.), and trifunctional polyether with trade name TEP-240 (hydroxyl value 23 mgKOH/g, Mn = 7300, Tianjin Third Petrochemical Co. Ltd.) were dried under vacuum at 90 °C to remove water. Dimethyl terephthalate (DMT), AR, 99.9%, Mn = 194.18, white powder was purchased from Tokyo Chemical Industry Co., Ltd. Hydrazine hydrate (AR, 80%, Mn = 50.06, colorless liquid) was purchased from Tianjin Chemical Co. Ltd. Diacetone alcohol (AR, Mn = 116.16, colorless liquid) was purchased from Sinopharm Chemical Reagent Co. Ltd. Glacial acetic acid (AR, Mn = 60.05, colorless liquid) was purchased from Nanjing Chemical Reagent Co. Ltd. Dibutyltin dilaurate (DBTDL, AR, 95.0%, Mn = 631.57, colorless oily liquid) was purchased from the Tianjin Chemical Reagent factory. Dimethyl sulfoxide (DMSO, AR, Mn = 78.13, colorless liquid) and N,N-dimethylformamide (DMF, AR, 99.5%, Mn = 73.09, colorless liquid) solvents were purchased from Tianjin Fuyu Fine Chemical Co. Ltd.

Purification process and particle size determination for natural melanin nanoparticles

The entire purification process is shown in Fig. 1a. Every 10 g of natural MNs extracted from fresh cuttlefish was first washed with 200 g of deionized water at a high mechanical stirring rate of 1500 rpm for 30 min Then, the black suspension was placed in an ultrasonic disperser for 30 min. These two steps were used to completely disperse and dissolve inorganic salts or other impurities into water. Third, the MNs were centrifuged at a high speed of 20,000 rpm to completely separate MNs from inorganic salts and most of soluble organic matter, which was dissolved in the supernatant liquid. The above three steps were repeated 5 times, and high purity MNs were finally obtained by vacuum dehydration at 50 °C for 7 days.

The particle size and size distribution of the MNs were determined by a Marvin diameter (Zeta sizer Nano ZS90). The MNs were dispersed by ultrasonication in water for 10 min; 90° dynamic light scattering was used to determine the hydration kinetic diameter of the MNs. As shown in Fig. 1b, there was only one peak in the curve, indicating that the particle size distribution was uniform. The particle size distribution of the MNs was 100–450 nm, of which the 400 nm occupied the largest proportion.

Synthesis of the acylhydrazone compound

The acylhydrazone compound (named AAD), which is a hydroxyl terminated chain extender in PU, was synthesized using terephthalic dihydrazide and diacetone alcohol. First, terephthalic dihydrazide was synthesized by dissolving 11.65 g (0.06 mol) DMT in 60.00 g ethanol and 12.00 g (0.24 mol) hydrazine hydrate at 80 °C for 2 h. The synthesized terephthalic dihydrazide was filtered under reduced pressure, washed 3 times with absolute ethanol and dried under vacuum to a constant weight to yield a light yellow powder, yield: 13.55 g, 87.5%. FTIR (KBr): wave number = 3327, 3050, 1607, 1541, 1491, 1341, 1103, 928, 737, 714, 639, 497, 436 cm^{-1}. ^{1}H-NMR (300 MHz, DMSO-d_6, δ): 9.87 (2H, –NH–), 7.87 (4H, Ar-H), 4.51(2H, –NH_2). The detailed synthetic information is presented in Fig. 4.

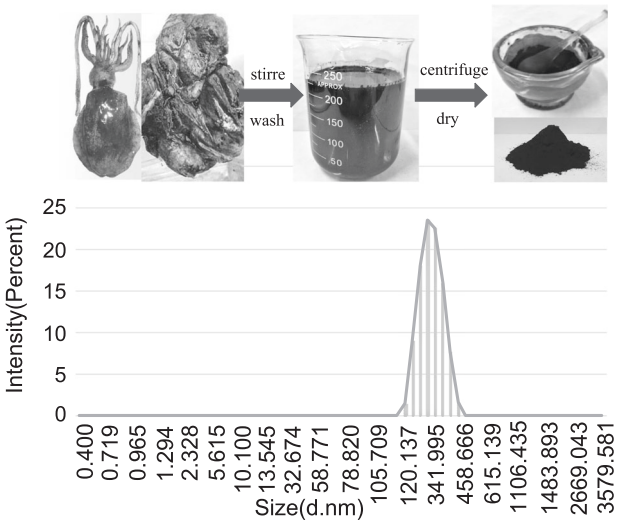

Fig. 1 Purification process and size distribution according to the intensity of MNs

Then, 19.42 g (0.1 mol) terephthalic dihydrazide was dissolved in 70.00 g acetic acid and reacted with 23.23 g (0.2 mol) diacetone alcohol under ambient conditions for 4 h. Finally, the resulting product, AAD, was filtered under reduced pressure, washed with deionized water and dried under vacuum to a constant weight. White powder, yield: 33.2 g, 85%. FTIR (KBr): wave number = 3329, 3182, 2969, 2540, 2358, 1658, 1620, 1562, 1370, 1323, 1164, 1056, 926, 704 cm^{-1}. ^{1}H-NMR (300 MHz, DMSO-d_6, δ): 11.98 (2H, –NH–), 8.00 (4H, Ar-H), 6.05 (2H, –OH), 2.45 (4H, –C–CH_2–), 2.02 (6H, –N=C–CH_3–), 1.25 (12H, –C–CH_3). The detailed synthetic information is presented in Fig. 5.

Synthesis of a self-healing cross-linked PU and natural melanin nanoparticle-modified self-healing cross-linked PU

First, 20.02 g (0.08 mol) of MDI-50 was added to a three-necked flask; then, 40.00 g (0.04 mol) of PCL-210 was added dropwise to the MDI-50, and the whole dropping process was controlled within 10 min. The ratio of hydroxyl groups to isocyanate groups in this system was 1: 2. Then, 0.5 wt% of DBTDL was added to the system and evacuated at 65 °C at a stirring rate of 250 rpm. The reaction was carried out for 2 h to generate an –NCO group terminated prepolymer named pre-PU1 (–NCOwt% = 5.59%). Similarly, the above reactive steps were repeated using 7.50 g (0.03 mol) of MDI-50 and 73.0 g (0.01 mol) of TEP-240 to synthesize another –NCO group terminated prepolymer, pre-PU2 (–NCOwt% = 1.56%). These reaction processes are shown in Scheme 1, step 1.

Second, 5.36 g (0.027 mol –OH) AAD dissolved in 15 g DMSO was reacted with a mixture of 15 g Pre-PU1 and 20.12 g pre-PU2. The mole ratio of hydroxyl groups to isocyanate groups was 1:1. After 30 min of high speed stirring (350 rpm), the viscous resin was poured into the open glass mold. The original self-healing cross-linked polyurethane (named PU-0) was obtained by curing for 12 h at 60 °C. (Scheme 1, step 2)

Finally, the reactive groups in MNs (hydroxyl, amino, etc.) were reacted with the –NCO groups in pre-polyurethane (pre-PU1 and pre-PU2) to form chemical cross-links, and self-healing polyurethanes modified with

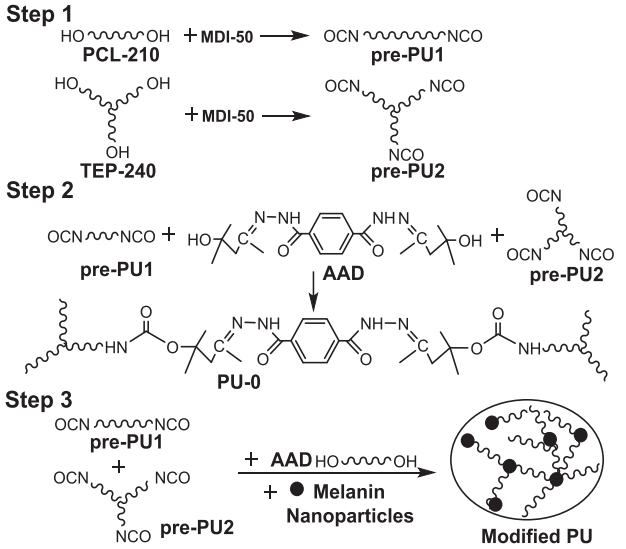

Scheme 1 Synthetic mechanism for the original PU (PU-0) and modified PU

Table 1 MNs/AAD content in modified PUs

Modified PU	Content of MNs (wt%)	MNs (g)	AAD (g)
PU-0	0.0	0.00	5.36
PU-0.5	0.5	0.18	5.16
PU-1.0	1.0	0.35	4.95
PU-1.5	1.5	0.53	4.75
PU-2.0	2.0	0.70	4.55
PU-2.5	2.5	0.88	4.34

The reactive group content in the MNs was 6.0 mmol/g, proved in "Results and discussion"

different mass fraction of MNs (0.5, 1, 1.5, 2, and 2.5 wt%) were synthesized and named PU-0.5, PU-1.0, PU-1.5, PU-2.0, and PU-2.5, respectively, based on the above self-healing cross-linked polyurethane system (Scheme 1, step 3). The specific contents of AAD and MNs in modified self-healing PUs were adjusted to obtain a better cross-linked self-healing PU, as shown in Table 1.

Characterizations

To determine the exact molecular structure of the MNs, the infrared spectra and content of the reactive groups were investigated. The reactive groups are groups that can react with isocyanate groups. Every gram of MNs was added to a different quality gradient of MDI-50 (0.1–0.8 g, with 0.8–6.5 mmol of –NCO), which was in the range of the reference contents [25]. The content of reactive groups on every gram of MNs was determined by the exact amount of MDI-50 observed in the infrared spectrum of MNs/MDI-50.

The morphologies of the MNs and their dispersion and adhesion in the PUs were observed using a scanning electron microscope (JSM-7500F) and transmission electron microscope (JEM-2100) from a Japanese electronics company.

To verify the target products synthesized in our work, they were confirmed by Infrared (Bruker, VERTEX70) and ^{1}H-NMR (Bruker AC500) spectroscopy.

To verify the cross-linked structures of MNs/PU, DSC (TA, Q20. 10 °C/min, N_2 atmosphere), the equilibrium swelling ratio (SR) and gel content ratio (GR) at ambient temperature were obtained and analyzed. SR and GR were investigated by the following two formulas:

$$\mathrm{SR} = \frac{(w_1 - w_0)}{w_0} \times 100\% \quad (1)$$

$$\mathrm{GR} = \frac{w_2}{w_0} \times 100\% \quad (2)$$

where w_0, w_1, and w_2 are the weights of the original sample, the swelling sample, and the drying sample, respectively. The solvent was DMF, and the drying process was carried out in a vacuum oven at 80 °C.

Mechanical property measurements were performed on a Tensile Test Machine (Zwick/005, Germany, ISO527-2) using a stretching speed of 100 mm/min.

To characterize the self-healing ability, the self-healing efficiency was calculated according to the ratio of the two important physical quantities in Tensile Test, and the formulas are as follows:

$$R(\sigma) = \frac{\sigma_1}{\sigma_0} \times 100\% \quad (3)$$

$$R(\varepsilon) = \frac{\varepsilon_1}{\varepsilon_0} \times 100\% \quad (4)$$

where σ_0 and σ_1 are the tensile strength of the original samples and self-healing samples, respectively. ε_0 and ε_1 are the elongation at breaking points of the original samples and the self-healing samples, respectively. The best self-healing time for the self-healing PU in this paper was 24 h according to our previous study [33], so tensile tests were carried out for 12 and 24 h for the self-healing samples.

Results and discussion

Analysis of the infrared spectra, content of reactive groups, and particle size of the melanin nanoparticles

In the spectrum presented in Fig. 2, 3361 cm^{-1} is very likely the stretching vibration absorption peak of $–NH_2$ or –OH. Since the stretching vibration peaks of double bonds, such as –C=C, –C=N, –C=O, –N=O and benzene rings ($\sigma_{C=C}$), occur from 1690 to 1500 cm^{-1}, the peak at 1570 cm^{-1} is

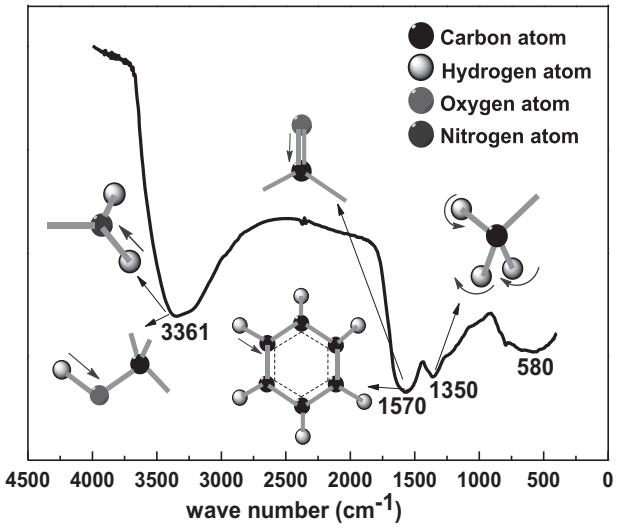

Fig. 2 Infrared spectra of MNs

most likely the stretching vibration peak of –C=O. The weak peak at 1350 cm^{-1} belongs to a saturated hydrocarbon vibration absorption peak or a –C–H in-plane bending vibration absorption peak. Additionally, the peak at 580 cm^{-1} is assigned as a vibrational absorption peak of carbon skeletons in the fingerprint region. Amino groups ($–NH_2$, –NH–) and –OH are the main reactive groups of MNs, as indicated by the strength of the peaks. We can see that the characteristics of the MNs' infrared spectra, wide and diffused, are consistent with the common characteristics of biomacromolecules.

In Fig. 3a, 2258 cm^{-1} is the infrared absorption peak of the –NCO groups, which was in excess in the system containing 1 g MNs and 0.8 g of MDI-50, while there are no –NCO groups in the system containing 1 g MNs/0.7 g MDI-50. It is roughly estimated that 1 g of MNs would completely react with 0.75 g MDI-50, so the reactive group content (–OH, –NH–, $–NH_2$) of MNs was 6.0 mmol/g. Obviously, heat and gas were released over the course of the MNs/MDI-50 reaction to support the high activity of MNs as a reactive filler, and a video of the reaction process is provided in the Supporting Information. Additionally, evidence for the reaction between the MNs and MDI-50 is provided in the SEM and TEM images in Fig. 3. Fig. 3b shows that the MNs were spherical in shape and approximately 100–400 nm in size. The particle size was similar to that obtained according to the Marvin diameter (Fig. 1b). Compared to the original picture of the MNs shown in Fig. 3b, some substances adhered to the surface, as shown in Fig. 3c, which was considered to be chemical cross-linking between the MNs and PU. This result can help explain why MNs can improve the mechanical properties of polyurethane.

Analysis of the synthetic products

Synthetic information for terephthalic dihydrazide

From the black curve (1) shown in Fig. 4b, the stretching vibration absorption peak of –C=O in DMT appeared at 1730 cm^{-1}. The anti-symmetric stretching vibration absorption peak of C–O–C in the ester group appeared at 1243–1100 cm^{-1}. The stretching vibration absorption of $–CH_3$ appeared at 2956 cm^{-1}. The peaks at 1278 and 1109 cm^{-1} were assigned to the asymmetric and symmetrical in-plane bending vibration absorption peak of $–CH_3$, respectively. In the red curve (2) shown in Fig. 4b, symmetrical and antisymmetric stretching vibration absorption peaks appeared at 3050 and 3320 cm^{-1}, respectively, and were assigned to the $–NH_2–$ of the hydrazide group. The stretching vibration absorption band of –C=O– in the terephthalic dihydrazide appeared at 1631 cm^{-1}. The disappearance of the absorption peaks of $–CH_3$ and C–O–C– and the presence of absorption peaks of –NH– indicate that the terephthalic dihydrazide was fully synthesized.

The ^{1}H-NMR signals shown in Fig. 4c were assigned as follows: $\delta = 9.85$ ppm for 2 protons from the –NH– group (as indicated by label a). $\delta = 7.87$ ppm for 4 protons from the benzene ring (as indicated by label b). $\delta = 4.51$ ppm for 4 protons from the $–NH_2–$ group (as indicated by label c). At the same time, terephthalic dihydrazide was fully synthesized, as indicated by the peak area ratio, a:b:c = 1:2:2.

Synthetic information for AAD

In the black curve (1) shown in Fig. 5b, the stretching vibration absorption peaks of C=O and O–H in diacetone alcohol were assigned to 1703 and 2990 cm^{-1}, respectively. The acylhydrazone bond in AAD was obtained by the reaction between the ketone carbonyl group and hydrazide group. The disappearance of the absorption peaks of the ketone carbonyl group indicates that the acylhydrazone bond was fully synthesized. In the blue curve (3) shown in Fig. 5b, there are no absorption peaks for ketone carbonyl group in the AAD infrared spectrum. However, the stretching vibration absorption peak of C=O in the acylhydrazone bond was in the range of 1607–1579 cm^{-1}. Furthermore, the stretching vibration absorption peaks of C=N and O–H appear at 1620 and 3182 cm^{-1}, respectively.

The ^{1}H-NMR signals shown in Fig. 5c, were assigned as follows: $\delta = 11.98$ ppm for 2 protons from the –NH– group (as indicated by label a). $\delta = 8.00$ ppm for 4 protons from the benzene ring (as indicated by label b). $\delta = 6.05$ ppm for 2 protons from the –OH group (as indicated by label c). $\delta =$ 3.35 ppm for the absorption peak of the solvent (D_2O). $\delta =$ 2.45 ppm for 4 protons from the $–C–CH_2–$ group (as indicated by label d). $\delta = 2.02$ ppm for 6 protons from

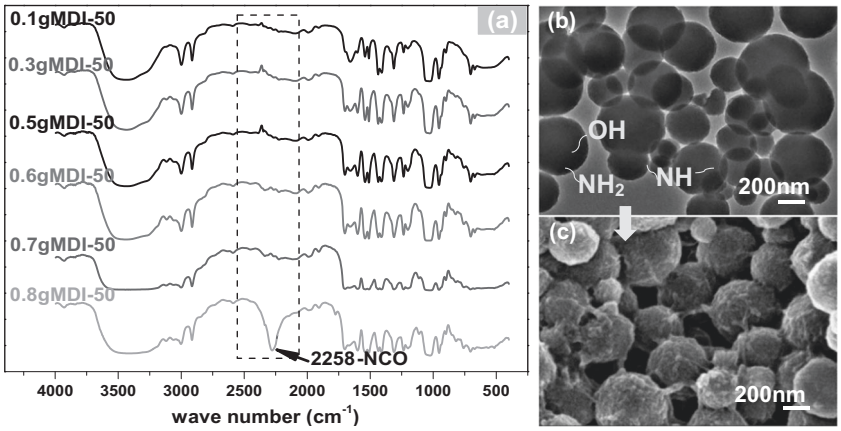

Fig. 3 **a** Infrared spectra of different masses of MDI-50 and MNs, **b** TEM image of MNs, and **c** SEM image of melanin-PU nanohybrids

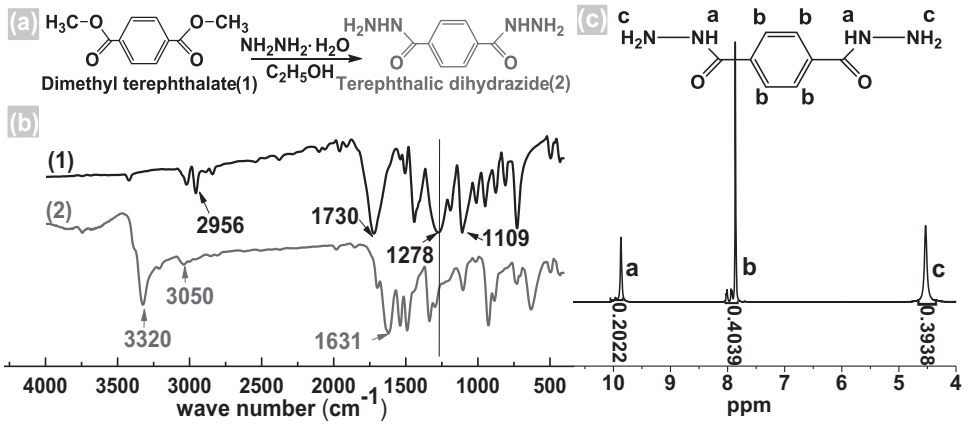

Fig. 4 Synthetic information of the **a** synthetic mechanism, **b** infrared spectra, and **c** ^{1}H-NMR spectra of terephthalic dihydrazide

the –(N=C)–CH_3– group (as indicated by label e). δ = 1.25 ppm for 12 protons from the –C–CH_3– group (as indicated by label f). The peak area ratio agrees with the acylhydrogen atom ratio in the target product.

Infrared spectra of PU-0/0.5/1.0/1.5/2.0/2.5

As seen in Fig. 6, the disappearance of the characteristic absorption peak of –NCO (2258 cm^{-1}) was used as a criterion to establish that the reaction among pre-PU1, pre-PU2, AAD, and MNs was completed. The stretching vibration absorption peaks of –NH– in carbamate groups appeared at 3380 cm^{-1}. With the addition of MNs, the stretching vibration absorption peak of –NH– in the carbamate groups in modified self-healing PUs formed by the reactive groups on the MNs and the –NCO groups were diffuse, which is related to the natural properties of MNs. The peak at 2940 cm^{-1} was assigned as the –C–H stretching vibration of the benzene rings from ADD. The amount of AAD decreased, while the amount of MNs increased from PU-0.5 to PU-2.5. This result can be explained by the fact that more benzene rings were included in the MNs, which is consistent with the infrared spectra of the MNs shown in Fig. 2. The stretching vibration absorption peak of C=O in the carbamate groups appeared at 1735 cm^{-1}, the intensity of which increased with the increase in the MN content. The stretching vibration absorption peak of C=N in the acylhydrazone bonds appeared at 1535 cm^{-1}. The peaks at 1222 and 1101 cm^{-1} were assigned to the absorption peaks of single-key, such as C–C, C–N, or C–O. Their absorption peaks in modified PUs were stronger than those of PU-0 due to the contribution of the single bonds provided by the MNs.

Evaluation of distribution and micro-behavior of MNs by SEM

As shown in Fig. 7, the shape of the MNs in modified PUs is no longer a regular spherical shape. The irregular shape resulted from the presence of adhesives on the surface of the MNs, which were chemical cross-links formed by the reaction between PU and MNs. Presented at a lower content (less than or equal to approximately 1.5 wt%) in the matrix, the distributions of MNs in modified PUs were uniform, and no agglomeration occurred, as shown in Fig. 7a–c. Their average size was 100–500 nm. MNs with a higher content (2.0 and 2.5 wt%) distributed in modified PUs are seen in

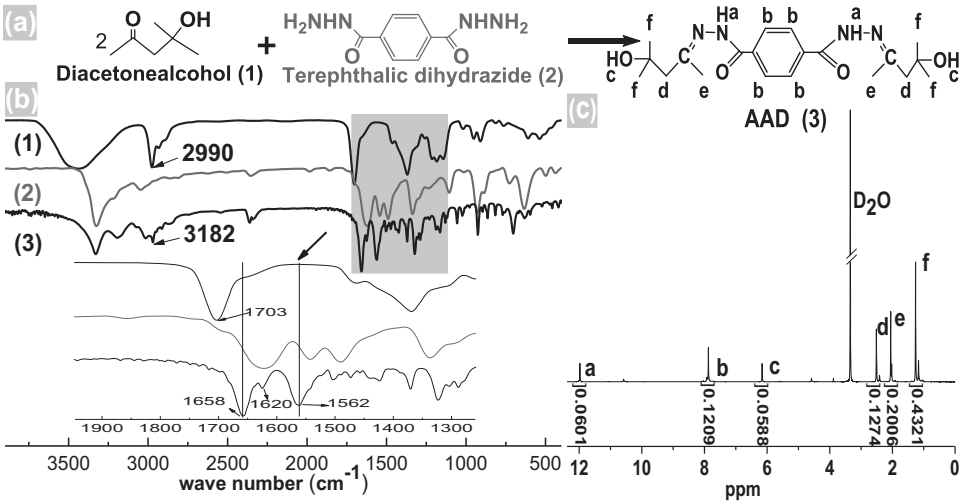

Fig. 5 Synthetic information of the **a** synthetic mechanism, **b** infrared spectra, and **c** ^{1}H-NMR spectra of AAD

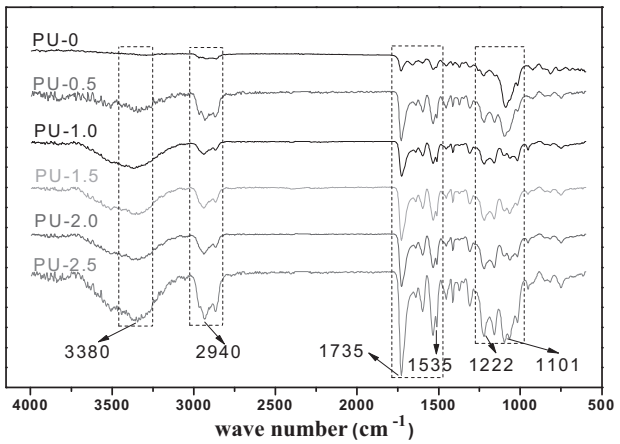

Fig. 6 Infrared spectra of PU-0/0.5/1.0/1.5/2.0/2.5

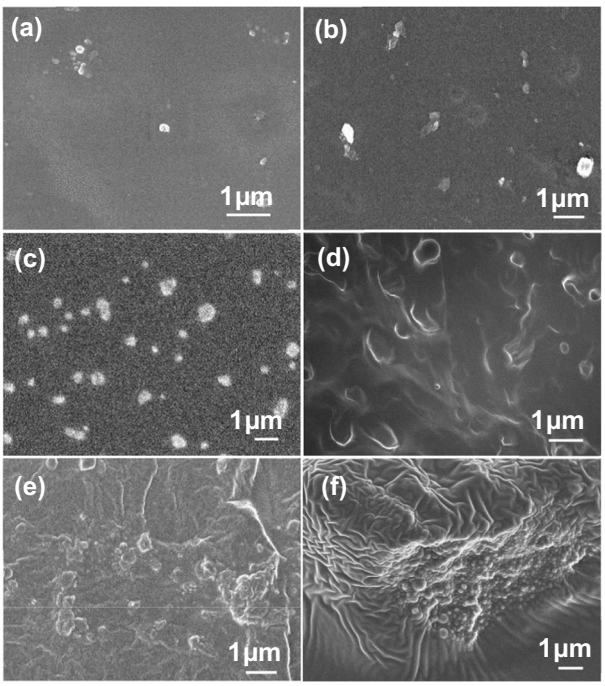

Fig. 7 SEM images of the distribution of MNs in **a** PU-0.5, **b** PU-1.0, **c** PU-1.5, **d** PU-2.0, and **e** PU-2.5 and **f** the agglomeration of MNs in PU-2.5

Fig. 7d, e, respectively, which shows greater agglomeration in the matrix. The size of the aggregates reached 1 μm. The detailed SEM image of MN agglomeration is shown in Fig. 7f. There is obvious shrinkage, which causes harmful internal defects. A large amount of MNs will lead to their predominant reaction with the –NCO group in PU, leading to agglomerations due to its higher reactive activity compared with AAD. It can be concluded from the SEM images that the natural nanoparticles, MNs, are well distributed in the PU matrix by ultrasonic dispersion during the synthetic process when their mass percentage does not exceed 1.5 wt%.

Cross-linked structure characterizations

DSC characterization

As seen in Fig. 8, there are two inflection points in the DSC curve, which were assigned as the glass transition temperatures for the soft and hard segments of the matrix, which were named T_{g1} and T_{g2}, respectively. The glass transition temperature (T_g) values were negative, so the cross-linked polyurethanes were in a high elastic state under ambient conditions owing to the properties of the elastomer. From the trend in the curve shown in Fig. 8, it is observed that with the increase in the MN content in the polyurethane matrix, T_{g1} decreases (from −39.56 °C to −56.54 °C) and he T_{g2} increases (from 62.26 °C to 87.72 °C).

Since the T_g of the polyurethane depends on the flexibility of the polyurethane segment, the lower the T_g, the more flexible the segments. The larger the gap between T_{g1}

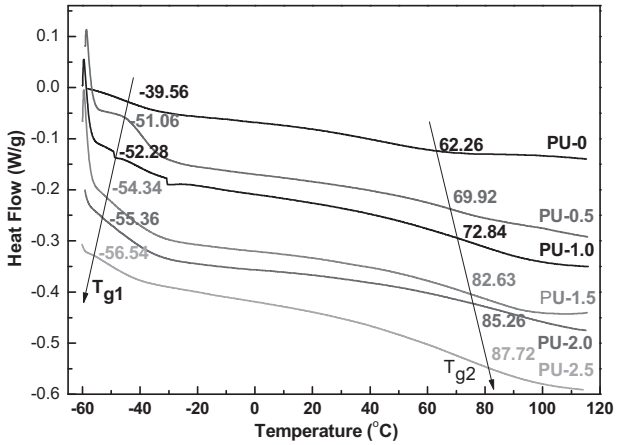

Fig. 8 DSC curves of PU-0/0.5/1.0/1.5/2.0/2.5

and T_{g2}, the greater the separation between the soft and hard segments. The fact that the modified self-healing polyurethane had a lower T_{g1} and a higher T_{g2} showed that the MNs, on one hand, functioned as nanofillers to disorder the overall arrangement of the polyurethane segments and enhanced the space and capacity of the segment movement. On the other hand, the MNs acted as chemical cross-linking points in the polyurethane system that can react with the hard segments to hinder their movement.

Analysis of the equilibrium swelling ratio and gel content

In Fig. 9a, the original samples roughly had a circular shape ($d = 10$ mm). The volumes of all of the samples increased during the swelling process, while their overall structure remained intact, indicating that they possessed better cross-linked structures. The diameters of the swelling samples PU-0/0.5/1.0/1.5/2.0 were approximately 17, 17, 19, 15, and 19 mm, respectively. PU-1.5 had the smallest swelling volume and the most regular shape, which indicates that it had a strong cross-linked structure. The edges of the swelling sample PU-2.5 were gel-like and deformed in morphology. It can be intuitively seen that the self-healing PUs modified with 1–1.5 wt% MNs showed a more closely cross-linked structure. However, an excessive (exceeding 2 wt%) MN content caused a swelling–yielding behavior, and their segments gradually loosened.

From the data shown in Fig. 9b and calculated by formulas (1) and (2), we can see that with the increase in MNs in the PU matrix, the GR initially increased and then decreased, indicating that an appropriate amount of MNs can form good chemical cross-linking in this system compared to PU-0. Additionally, modified self-healing PUs with 1 and 1.5 wt% MNs (PU-1.0 and PU-1.5, respectively) had a lower SR. However, the SR and GR of PU-2.5 were lower than those of the other samples, which can be attributed to too a large number of MNs becoming a physical stress and causing a concentration point that increases the separation between the soft and hard segments, further loosening the system segments, which can be confirmed by their swelling diagrams.

Based on above analysis of the swelling behavior and gel content, we conclude that the optimum cross-linking structure can be obtained by adding approximately 1.5 wt% MNs, which worked as functional chemical filler, to self-healing polyurethane.

Evaluation of mechanical properties in terms of the tensile test

The stress–strain curves of the PUs were recorded and are shown in Fig. 10a. The numerical features σ and ε of PU-0 were in accordance with the mechanical properties of soft elastomer materials. With the increasing MN content, the overall mechanical properties initially increased and then decreased. PU-1.0 and PU-1.5 modified with 1 and 1.5 wt% MNs, respectively, showed better mechanical properties. Their σ and ε values were much higher than those of PU-0. The σ value of PU-0.5 and PU-2.0 increased slightly, while the ε value greatly decreased. Modified with 2.5 wt% MNs, PU-2.5 had worse mechanical properties than before modification.

We can see that the improvement in the mechanical properties of polyurethanes was not directly proportional to the addition of MNs. The above phenomenon can be explained by the mechanism by which MNs enhance Pus, as shown in Fig. 10b. An appropriate amount of MNs added to a PU matrix can form orderly chemical cross-linking points combined with AAD to enhance the mechanical properties. However, excessive MNs give rise to their high reactivity toward magnetization. PUs modified with MNs, the content of which exceeded 2 wt%, showed a large performance degradation in this work. It is a fact that most of the MNs were wrapped in the surrounding polyurethane matrix, which acted more like a physical filler than as chemical cross-links. At the same time, limited chemical cross-links did not have a positive effect in this case. Structural defects resulting from the stress concentration points were liable to cause the material deformation and failure.

Quantitative characterization of the self-healing efficiency

As shown in Table 2, the resulting valid data obtained from the tensile test were processed and compared. The sequence of $R(\sigma)$ from high to low was PU-0 (90.12%), PU-1.0 (89.49%), PU-1.5 (82.22%), PU-0.5 (73.98%), PU-2.5 (73.42%), and PU-2.0 (63.96%), and the sequence of $R(\varepsilon)$ from high to low was PU-1.5 (99.58%), PU-1.0 (90.69%), PU-0 (90.37%), PU-0.5 (86.19%), PU-2.0 (83.88%), and

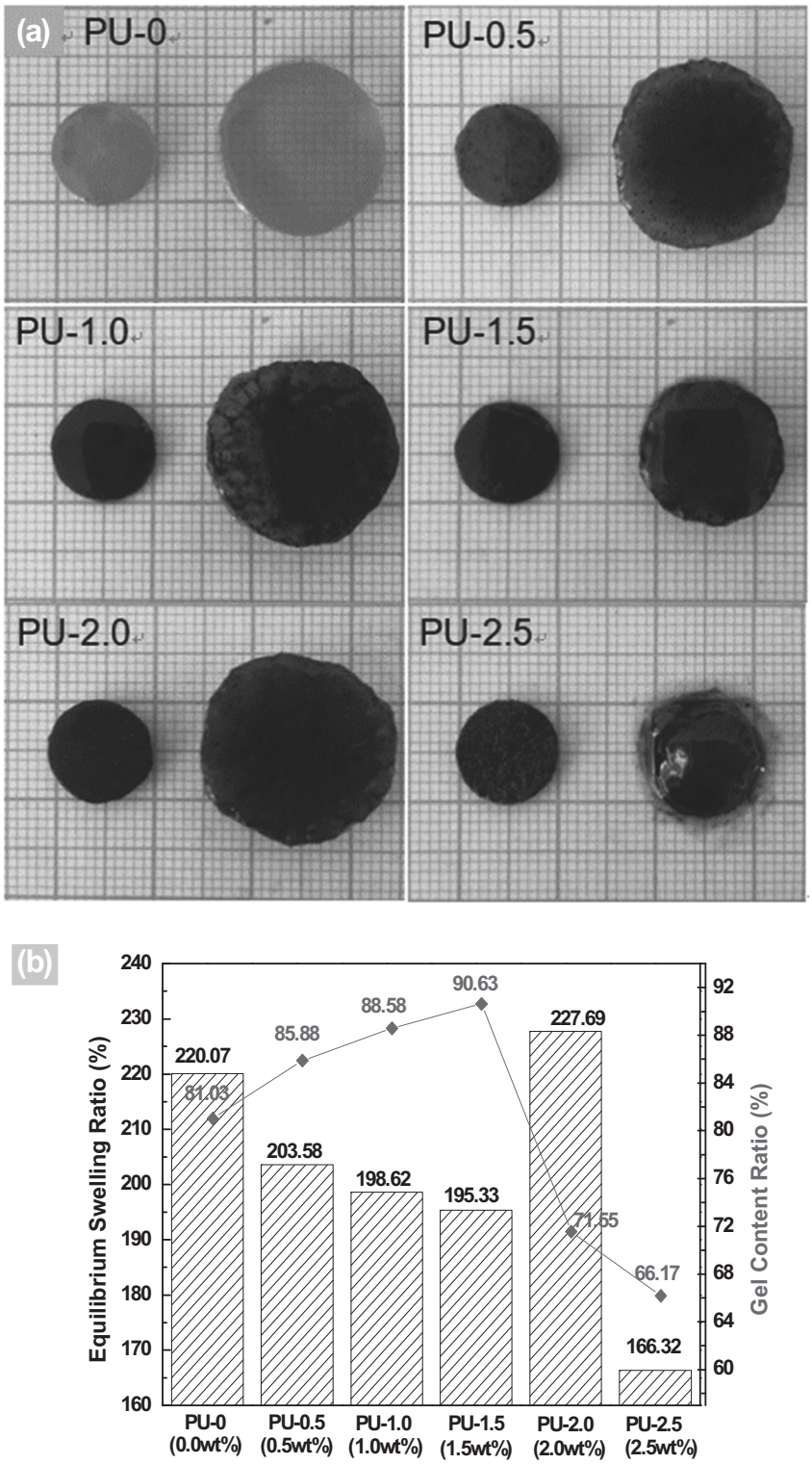

Fig. 9 **a** Morphology comparison of PU-0/0.5/1.0/1.5/2.0/2.5 before and after swelling and **b** the gel content ratio and equilibrium swelling ratio

PU-2.5 (51.76%). PU-0, PU-1.0, and PU-1.5 were ranked in the top three. PU-1.5 exhibited a good performance, and its self-healing properties were not sacrificed, while its mechanical properties were simultaneously improved. We can even see that the self-healing efficiency, defined by R (ε), of PU-1.5 was higher than that of PU-0. A surprising discovery was that the addition of MNs, which was intended to improve the initial mechanical properties of PU, improved the self-healing performance of the self-healing PU to a certain extent.

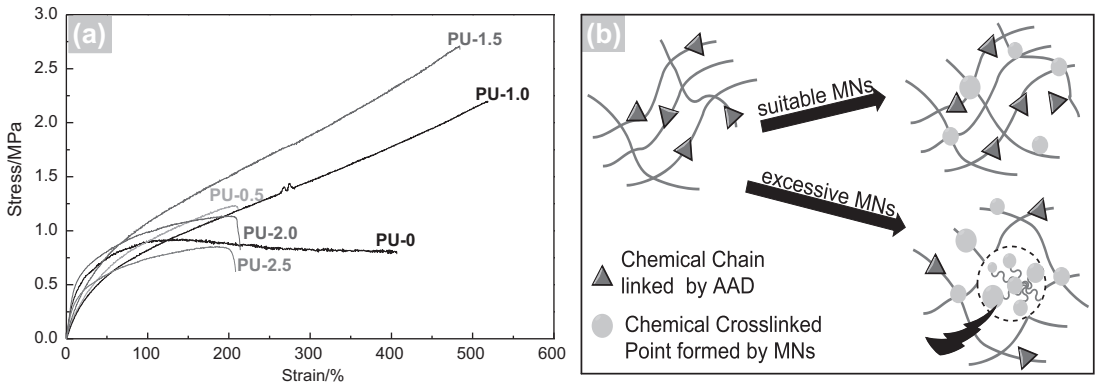

Fig. 10 **a** Tensile test curves of PU-0/0.5/1.0/1.5/2.0/2.5 and **b** the reinforcement mechanism

Table 2 Records of tensile strength (σ/MPa) and elongation-at-break (ε/%) for self-healing for 12 and 24 h

Tensile test item	σ_0	ε_0	Self-healing for 12 h				Self-healing for 24 h			
			σ_1	$R(\sigma)$	ε_1	$R(\varepsilon)$	σ_1	$R(\sigma)$	ε_1	$R(\varepsilon)$
PU-0	0.81	405	0.61	75.31%	242	59.75%	0.73	90.12%	366	90.37%
PU-0.5	1.23	210	0.92	74.79%	124	59.04%	0.97	73.98%	181	86.19%
PU-1.0	2.19	518	1.64	61.89%	422	83.86%	1.96	89.49%	458	90.69%
PU-1.5	2.75	483	2.03	75.18%	470	99.36%	2.22	82.22%	471	99.58%
PU-2.0	1.11	211	0.62	55.85%	165	78.19%	0.71	63.96%	177	83.88%
PU-2.5	0.79	199	0.34	43.04%	82	41.20%	0.58	73.42%	103	51.76%

$R(\sigma)$ and $R(\varepsilon)$ were calculated according to formulas (3) and (4)

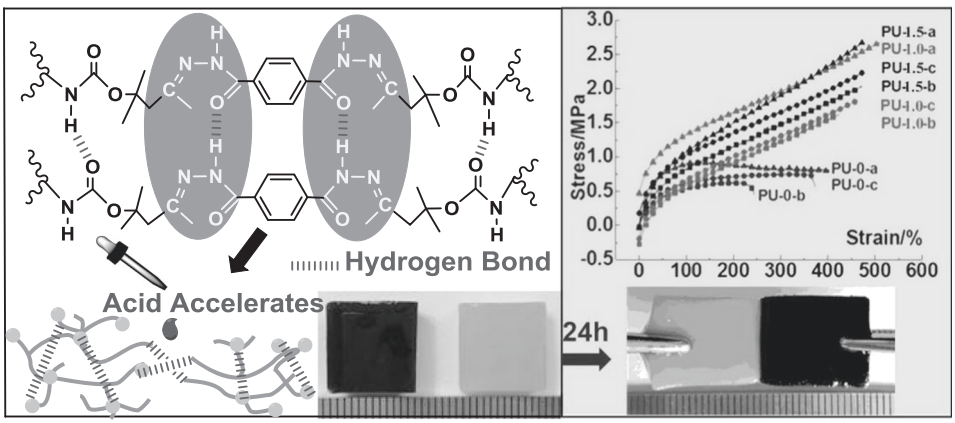

Fig. 11 Self-healing mechanism, stretching diagram, and tensile curves of modified PUs. **a** Original samples and samples with a self-healing time of **b** 12 h and **c** 24 h

Therefore, for the study of the self-healing ability of PUs with better mechanical strength, only two modified self-healing PUs (PU-1.0 with 1 wt% MNs and PU-1.5 with 1.5 wt% MNs) were selected as to contrast with PU-0 in the subsequent experiments. The tensile curves of the self-healing samples PU-0, PU-1.0, and PU-1.5 are shown in Fig. 11.

Analysis of the self-healing mechanism

It should be noted that a high self-healing efficiency was achieved by dropping glacial acetic acid (50%, a drop of approximately 0.05 ml) into the sample cracks to impel the dynamic reversible reaction of the acylhydrazone bond. The self-healing mechanism, on one hand, can repair broken segments by the dynamic exchange reactions of the acylhydrazone bonds of AAD. Polymer chains with a benzene ring in AAD and MNs tend to be more stable conjugate structures to force the repair of cracks. On the other hand, the micro-cracks rapidly heal due to the contribution of the large number of hydrogen bonds provided by the supra molecular effects of the acylhydrogen bonds between the PU segments. Moreover, there were enough chemical cross-linking points formed by the MNs and isocyanate groups in

the modified polyurethane matrix, which provided multiple hydrogen bonds to support the polyurethane network, to further help repair cracks. All of these mechanisms can be reasonably explained by Fig. 11. It can also be seen in Fig. 11 that when two different self-healing polyurethane specimens were placed together, after 24 h of self-healing, they were completely repaired without being separated under a certain tensile stress condition. Furthermore, they can be stretched to at least 16 mm while maintaining the integrity of their shape.

We can see from the tensile curves shown in Fig. 11 that the σ values of the three self-healing samples cannot reach the values of the original samples, but their ε values can basically be restored to their original values. Among them, the ε value of PU-1.0 was higher than that of PU-1.5, but its mechanical strength (represented by σ) was lower and its self-healing effect was poor. It can be inferred from the red and black curves that the gap between curve PU-1.0-a and curve PU-1.0-b or curve PU-1.0-c was larger than that of PU-1.5. Therefore, 1.5 wt% MNs was found to be best for achieving the best performance.

Conclusions

In this paper, the self-healing PU based on reversible covalent acylhydrazone bonds showed a high self-healing efficiency, and its σ value was able to be restored to 90.12% after self-healing for 24 h. However, its application was limited by its poor mechanical properties, of which the σ and ε values were 0.81 MPa and 405.44%, respectively. It was found by a series of characterizations that modification of the self-healing PU by 1.5 wt% MNs was better for enhancing its mechanical properties compared to other MN contents. In addition to the mechanical properties (defined by σ and ε), its self-healing performance was also improved by the chemical cross-links and microphase separations in PU. MNs were added to PU materials both as a physical filler to adjust the microphase separation and to act as a chain extender to form chemical cross-links, which were confirmed by SEM, DSC, and the Tensile Test. Only the appropriate MN content yielded the best results by promoting the dynamic reactions of the acylhydrazone bond in the molecular chains of the whole system. The surplus was lost for MNs added to self-healing PU. In further studies, MNs may play a unique role in other fields due to their contributions to both the mechanical and self-healing properties of the self-healing PU described in this work.

Acknowledgements This work was supported by the National Natural Science Foundation of China (Grant No. 51103078).

Compliance with ethical standards

Conflict of interest The authors declare that they have no conflict of interest.

Publisher's note: Springer Nature remains neutral with regard to jurisdictional claims in published maps and institutional affiliations.

References

1. Krol P. Synthesis methods, chemical structures and phase structures of linear po]lyurethanes. Properties and applications of linear polyurethanes in polyurethane elastomers, copolymers and ionomers. Prog Mater Sci. 2007;52:915–1015.
2. Ferguson J, Ahmad N. Chemical structure and physical properties in polyester-based segmented polyurethanes. Eur Polym J. 1977;13:859–64.
3. Wu DY, Meure S, Solomon D. Self-healing polymeric materials, a review of recent developments. Prog Polym Sci. 2008;33:479–522.
4. Cho SH, White SR, Braun PV. Room-temperature polydimethylsiloxane-based self-healing polymers. Chem Mater. 2012;24:4209–14.
5. Wietor JL, Sijbesma RP. A self-healing elastomer. Angew Chem Int Ed. 2008;47:8161–3.
6. Imato K, Nishihara M, Kanehara T, Amamoto Y, Takahara A, Otsuka H. Self-Healing of Chemical Gels Cross-Linked by Diarylbibenzofuranone-Based Trigger-Free Dynamic Covalent Bonds at Room Temperature. Angew Chem Int Ed. 2012;51:1138–42.
7. Kalista SJ, Pflug JR, Varley RJ. Effect of ionic content on ballistic self-healing in EMAA copolymers and ionomers. Polym Chem. 2013;4:4910–26.
8. Jacob K. Repair or replacement, a joint perspective. Science. 2009;323:47–8.
9. Pramanik NB, Nando GB, Singha NK. Self-healing polymeric gel via RAFT polymerization and Diels–Alder click chemistry. Polymer (Guildf). 2015;30:1e8.
10. Deng G, Li F, Yu H, Liu F, Liu C, Sun W, et al. Dynamic hydrogels with an environmental adaptive self-healing ability and dual responsive sol–gel transitions. ACS Macro Letters. 2012;1:275–279.
11. Yoon JA, Kamada J, Koynov K, Monhin J, Nicolay R, Zhang Y, et al. Self-healing polymer films based on thiol–disulfide exchange reactions and self-healing kinetics measured using atomic force microscopy. Macromolecules. 2011;45:142–9.
12. Cong HP, Wang P, Yu SH. Stretchable and self-healing graphene oxide-polymer composite hydrogels, a dual-network design. Chem Mater. 2013;25:3357–62.
13. Ling J, Rong MZ, Zhang MQ. Photo-stimulated self-healing polyurethane containing dihydroxyl coumarin derivatives. Polymer (Guildf). 2012;53:2691–8.
14. Chung CM, Roh YS, Cho SY, Kim JG. Crack healing in polymeric materials via photochemical (2+2) cycloaddition. Chem Mater. 2004;16:3982–4.
15. Lehn JM. Dynamers, dynamic molecular and supramolecular polymers. Prog Polym Sci. 2005;30:814–31.
16. Xu Z, Zhao P, Chen Y, Deng G. Dynamic polymers containing one acylhydrazone linkage and dynamic behavior thereof(J). Polymer. 2013;54:2647–51.
17. Deng G, Tang C, Li F, Jiang H, Chen Y. Covalent cross-linked polymer gels with reversible sol− gel transition and self-healing properties. Macromolecules. 2010;43:1191–94.

18. Apostolides DE, Patrickios CS, Leontidis E, Kushnir M, Wesdemiotis C. Synthesis and characterization of reversible and self-healable networks based on acylhydrazone groups. Polymer International. 2014;63:1558–1565.
19. Spoljaric S, Salminen A, Luong N,D, Seppala J. Stable, self-healing hydrogels from nanofibrillated cellulose, poly (vinyl alcohol) and borax via reversible crosslinking. European Polymer Journal. 2014;56:105–17.
20. Dai X, Zhang Y, Gao L, Bai T, Wang W, Cui Y, et al. A Mechanically Strong, Highly Stable, Thermoplastic, and self-healable supramolecular polymer hydrogel. Advanced Materials. 2015;27:3566–71.
21. Ji S, Cao W, Yu Y, Xu H. Dynamic diselenide bonds: exchange reaction induced by visible light without catalysis. Angewandte Chemie International Edition. 2014;53:6781–85.
22. Li CH, Wang C, Keplinger C, Zuo JL, Jin L, Sun Y, et al. A highly stretchable autonomous self-healing elastomer. Nature chemistry. 2016;8:618–24.
23. Podsiadlo P, Kaushik AK, Arruda EM, Waas AM, Shim BS, Xu J, et al. Ultrastrong and stiff layered polymer nanocomposites. Science. 2007;318:80–3.
24. Yu X, Pan Y, Wang D, Yuan B, Song L, Hu Y. Fabrication and Properties of Biobased Layer-by-Layer Coated Ramie Fabric-Reinforced Unsaturated Polyester Resin Composites. Industrial & Engineering Chemistry Research. 2017;56:4758–67.
25. Gisselfält K, Helgee B. Effect of soft segment length and chain extender structure on phase separation and morphology in poly (urethane urea)s. Macromol Mater Eng. 2003;288:265–71.
26. Meuse CW, Yang X, Yang D, Hsu SL. Spectroscopic analysis of ordering and phase-separation behavior of model polyurethanes in a restricted geometry. Macromolecules. 1992;25:925–32.
27. Wang Y, Li T, Wang X, Ma P, Bai H, Dong W. Superior Performance of Polyurethane Based on Natural MNs. Biomacromolecules. 2016;17:3782–9.
28. Magarelli M, Passamonti P, Renieri C. Purification, characterization and analysis of sepia melanin from commercial sepia ink (*Sepia officinalis*)—Purificación, caracterización yanálisis de la melanina de sepia a partir de la tinta de sepia (*Sepia officinalis*). CES Med Vet Zootec. 2010;5:18–28.
29. Meredith P, Sarna T. The physical and chemical properties of eumelanin. Pigment Cell Res. 2006;19:572–94.
30. Albanese G, Bridelli MG, Deriu A. Structural dynamics of melanin investigated by Rayleigh scattering of Mössbauer radiation. Biopolymers. 1984;23:1481–98.
31. Abouzahr S, Wilkes GL. Structure property studies of polyester- and polyether-based MDI-BD segmented polyurethanes. Effect of one-vs.two-stage polymerization conditions. J Appl Polym Sci. 1984;29:2695–711.
32. Rekondo A, Martin R, de Luzuriaga AR, Cabanero G, Grande HJ, Odriozola I. Catalyst-free room-temperature self-healing elastomers based on aromatic disulfide metathesis. Materials Horizons. 2014;1:237–40.
33. Wei Y, Du X, Ma X, Zhao K, Zhang S, Bai Y. Synthesis and self-healing property of polyurethane modified with three-furyl diol. Polymer Bulletin. 2017;74:3907–22.